Geochemistry Geophysics Geosystems G3

Article
Volume 14, Number 12
24 December 2013
doi: 10.1002/2013GC004905
ISSN: 1525-2027

Published by AGU and the Geochemical Society

Frequency-dependent noise sources in the North Atlantic Ocean

Amandine Sergeant and Eléonore Stutzmann
Institut de Physique du Globe de Paris, Sorbonne Paris Cité, Université Paris Diderot, CNRS, F-75005 Paris, France (sergeant@ipgp.fr)

Alessia Maggi
Institut de Physique du Globe de Strasbourg, Université de Strasbourg/EOST, CNRS, Strasbourg Cedex, France

Martin Schimmel
Institute of Earth Sciences Jaume Almera, ICTJA-CSIC, Barcelona, Spain

Fabrice Ardhuin
Laboratoire d'Océanographie Spatiale, Ifremer, Plouzané, France

Mathias Obrebski
Laboratoire d'Océanographie Spatiale, Ifremer, Plouzané, France

Now at Lamont-Doherty Earth Observatory of Columbia University, Palisades, New York, USA

[1] Secondary microseisms are the most energetic waves in the noise spectra between 3 and 10 s. They are generated by ocean wave interactions and are predominantly Rayleigh waves. We study the associated noise sources in the North Atlantic Ocean by coupling noise polarization analysis and source mapping using an ocean wave model that takes into account coastal reflections. From the Rayleigh wave polarization analysis, we retrieve the back azimuth to the noise sources in the time-frequency domain. Noise source modeling enables us to locate the associated generation areas at different times and frequencies. We analyze the distribution of secondary microseism sources in the North Atlantic Ocean using 20 broadband stations located in the Arctic and around the ocean. To model the noise sources we adjust empirically the ocean wave coastal reflection coefficient as a function of frequency. We find that coastal reflections must be taken into account for accurately modeling 7–10 s noise sources. These reflections can be neglected in the noise modeling for periods shorter than 7 s. We find a strong variability of back azimuths and source locations as a function of frequency. This variability is largely related to the local bathymetry. One direct cause of the time-dependent and frequency-dependent noise sources is the presence of sea-ice that affects the amplitude and polarization of microseisms at stations in the Arctic only at periods shorter than 4 s.

Components: 8,061 words, 7 figures.

Keywords: noise sources; secondary microseism; North Atlantic Ocean; polarization.

Index Terms: 7255 Surface waves and free oscillations: Seismology.

Received 18 June 2013; **Accepted** 10 October 2013; **Published** 24 December 2013.

Sergeant, A., E. Stutzmann, A. Maggi, M. Schimmel, F. Ardhuin, and M. Obrebski (2013), Frequency-dependent noise sources in the North Atlantic Ocean, *Geochem. Geophys. Geosyst.*, *14*, 5341–5353, doi:10.1002/2013GC004905.

1. Introduction

[2] The dominant features of seismic noise are similar for stations everywhere on Earth including stations in polar areas. Seismic noise spectra display two peaks which correspond to the so-called primary (0.07–0.1 Hz) and secondary (0.1–0.33 Hz) microseisms. Primary or single frequency microseisms (SFM) are generated when ocean waves hit sloped coasts [*Hasselmann*, 1963] and their seismic waves have the same frequencies as the incident ocean waves. Secondary or double frequency microseisms (DFM) are more energetic and are generated by the interaction of ocean waves of similar frequencies and opposite directions [*Longuet-Higgins*, 1950]. The resulting seismic noise frequency is the double of that of the ocean waves. *Ardhuin et al*. [2011] showed that such ocean wave interactions can occur in three situations: within a single storm when the ocean wave directional spectra are broad (class I), close to a coast when the incoming ocean waves meet those reflected on the shore (class II), and finally, when a swell meets another swell or a wind sea (class III). The first successful attempt to model class I and class III seismic noise using an ocean wave model was performed by *Kedar et al*. [2008]. More recently, *Ardhuin et al*. [2011] have developed a more accurate wave model that can compute all three classes of noise sources. *Stutzmann et al*. [2012] showed that this wave model enables accurate modeling of the seismic noise spectra in various environments. Whereas *Bromirski et al*. [2013] consider that land stations record dominantly class II sources, *Stutzmann et al*. [2012] and *Obrebski et al*. [2012] presented a class III noise source in the North Atlantic Ocean recorded in France and another in the Pacific Ocean recorded all around the Pacific Ocean.

[3] The use of seismic data to determine the locations of the secondary microseism sources and their variation with time and frequency is a challenge. Indeed, secondary microseisms are predominantly composed of surface waves, and signal processing techniques such as beamforming or polarization analyses enable the determination of the source back azimuth [e.g., *Friedrich et al*., 1998; *Gerstoft and Tanimoto*, 2007; *Chevrot et al*., 2007; *Brooks et al*., 2009; *Koper et al*., 2010; *Schimmel et al*., 2011a; *Behr et al*., 2013]. Whereas beamforming requires a dense seismic network, polarization analyses can be performed on individual stations. Because surface waves propagate parallel to the Earth's surface, none of these methods enable the determination of the distance to the source. Furthermore, the exact source location is often difficult to determine by back projecting the source azimuth, because of the complexity of the secondary microseism excitation. Indeed, the source amplitudes vary with time and frequency, and the modulation of the sources varies with frequency, bathymetry, and the S-wave velocity in the crust [*Longuet-Higgins*, 1950].

[4] Seismic noise can be used as a monitoring tool to characterize sea states [*Bromirski et al*., 1999; *Bromirski and Duennebier*, 2002; *Aster et al*., 2010; *Ardhuin et al*., 2012] and also to investigate climate changes [*Stutzmann et al*., 2000; *Stehly et al*., 2006; *Aster et al*., 2008]. *Stutzmann et al*. [2009] showed that the decrease of primary and secondary microseismic noise at the GEOSCOPE station Dumont D'Urville (DRV) in Antarctica is correlated with nearby sea-ice formation. *Grob et al*. [2011] and *Tsai and McNamara* [2011] further showed that seismic noise can be used to monitor the sea-ice concentration close to the stations in Antarctica and Alaska, respectively. Using an ocean wave model, *Stutzmann et al*. [2012] modeled seismic noise recorded at DRV, and accurately reproduced the observations of *Stutzmann et al*. [2009] and *Grob et al*. [2011]: a decrease of short-period secondary microseism noise with increasing ice presence, suggesting that the corresponding noise sources are coastal, and no appreciable variation of the longer-period secondary microseisms, suggesting that the corresponding sources are far from the coast.

[5] We investigate seismic noise variability in the polar area around Greenland. The North Atlantic Ocean is an excellent site for analyzing secondary microseism sources. The ocean is small compared to large open oceans such as the Indian and Pacific Oceans, and therefore, seismic noise generated in the North Atlantic may be less attenuated over the shorter distances to the stations. Furthermore, many noise source studies have revealed seismic sources in this area. *Cessaro* [1994] and *Schulte-Pelkum et al*. [2004] analyze continuous data from North American and Norwegian arrays and report signals coming from the direction of the North Atlantic Ocean. By wide-angle triangulation of the measured secondary microseism azimuths, *Cessaro* [1994] shows the presence of noise sources along the coasts of New FoundLand near the Labrador Sea. *Kedar et al*. [2008] successfully modeled seismic noise in that area with a model that neglects coastal reflection (class II sources) and concluded that the strongest noise sources are

generated in deep ocean. They report persistent strong Rayleigh wave sources near the southern tip of Greenland. Their source model and seismic spectra are averaged over the entire microseism frequency band 0.14–0.3 Hz. Here, we investigate the frequency-dependent noise generation in the North Atlantic. The differences between our model and Kedar's model are that we include the class II sources and we adjust the ocean wave reflection coefficient as a function of frequency. We use stations in Greenland from the GLISN network (Greenland Ice-Sheet Monitoring Network, *Anderson et al*. [2009]) and stations in North America and Europe from global networks. We combine Rayleigh wave polarization analysis and source mapping from an ocean wave model to characterize the noise sources. We show that there is a strong variability of seismic noise sources as a function of frequency and that, similarly to Antarctica, sea-ice changes affect seismic noise only at short periods. We further show that stations in Northern Canada record long-period Pacific sources whereas Greenland stations only record regional sources.

2. Data and Methods

2.1. Polarization Analysis

[6] To locate secondary microseism sources over time, we perform a frequency-dependent polarization analysis of the seismic signal [*Schimmel and Gallart*, 2004; *Schimmel et al*., 2011b] in the frequency range 0.05–0.33 Hz. Polarization describes the particle ground motion at the receiver considering seismic records along the three directions (North-South, East-West, and vertical up). Microseisms are predominantly Rayleigh waves which have elliptical polarization. In the ideal case, this ellipse stands in the vertical plane which connects the sensor and the source. By estimating the direction of the incoming Rayleigh waves at each station, we obtain the azimuth to the noise source (back azimuth, BAZ) in the time-frequency domain.

[7] We use the S transform [*Stockwell et al*., 1996; *Ventosa et al*., 2008] for the time-frequency decomposition of each trace. The time window is scaled with the period of interest. Polarization attributes are the semimajor and semiminor axes of the ellipse that best fits the ground motion. They are determined through an eigen analysis of the cross spectra between the three components. The planarity vector is defined as the vector cross product between the time-frequency-dependent semimajor and semiminor vectors. The degree of polarization (DOP) is then computed as the projection of the instantaneous unit planarity vector on the mean planarity vector direction. The mean planarity vector is determined in a frequency-dependent moving window, and the DOP is an instantaneous quality measure based on the stability of an arbitrary polarization state with time. By weighting the DOP by the sine of the angle between the planarity vector and the vertical, we further select only the elliptically polarized signal in the vertical plane (see *Schimmel et al*. [2011b] for more details). The DOP is normalized, and DOP = 1 corresponds to a wave with a stable particle motion on an ellipse in the vertical plane. Hereafter, we select all signals with DOP larger than 0.75 and compare the measured back azimuth with the noise source maps.

[8] The propagation through the ocean continent boundary may modify the nature of the recorded signal. There can be mode coupling among the Rayleigh wave modes and among the Love wave modes, and also mode coupling between Rayleigh and Love waves. But the secondary microseism source corresponds to vertical forces at the ocean surface [*Gualtieri et al*., 2013]. Vertical force sources generate only Rayleigh waves and predominantly the fundamental mode of Rayleigh waves in the period range of interest (3–10 s). Waveform distorsion due to mode coupling should be less severe for the secondary microseisms than for earthquakes, which generate also Love waves and higher mode Rayleigh waves with larger amplitudes. Nevertheless, *Tanimoto et al*. [2006] showed that the relative excitation of the fundamental mode with respect to the higher modes can vary with the bathymetry at the source. This effect may become important at short period (3–5 s) and distort the waveform. If there is signal distortion, the number of detected polarized signals may decrease. Still, these detected elliptically polarized waves in a vertical plane are likely dominated by the stronger fundamental mode Rayleigh waves, which under the assumption of retrograde polarization provide the BAZ to the source area. Azimuth deviations due to heterogeneities such as the ocean continent boundary of about $\pm 20^\circ$ will not alter the results presented hereafter.

2.2. Noise Source Modeling

[9] As we cannot calculate the distance to the Rayleigh wave sources, we compare the source azimuths retrieved from the polarization analysis

with the noise sources predicted by a numerical wave model [*Ardhuin et al.*, 2011]. The source maps are computed for the same frequency range as that used for the polarization analysis. Our wave model takes into account the ocean wave coastal reflections. The model is computed with and without a spatially uniform coastal reflection. We obtain sources that correspond to any spatially uniform specific coastal reflection coefficient by a simple linear combination of the two models. To determine the coastal reflection coefficient R^2 adapted to the area of interest, we model seismic noise spectra at each station for a wide range of R^2.

[10] *Stutzmann et al.* [2012] express the power spectral density of the vertical displacement at the station location (λ, ϕ) and for a given seismic frequency f as:

$$F(\lambda,\phi,f)=\int_0^{2\pi}\int_0^{\pi}\frac{S(f)}{a\sin(\alpha)}P(f)\exp\left(\frac{-2\pi f a\alpha}{QU}\right)a^2\sin(\phi')d\lambda' d\phi' \quad (1)$$

where $S(f)$ is the DFM Rayleigh wave source located at the colatitude-longitude grid point (ϕ',λ'), a is the Earth's radius, α is the angular epicentral distance and $a^2\sin(\phi)d\lambda d\phi$ is the elementary surface area, U is the group velocity, and Q is the seismic attenuation. $P(f)$ is an empirical dimensionless parameter that takes into account the three-dimensional (3-D) propagation or local effect. *Stutzmann et al.* [2012] showed that this parameter can be neglected for the North Atlantic, and therefore, we use $P(f) = 1$. For modeling synthetic spectra, we need to adjust the product QU. Hereafter, we fix $U = 1.8$ km/s in the frequency band of interest and vary Q. The objective adjustment of the two parameters (Q, R^2) is performed by minimizing the difference between observed and modeled noise spectra for varying Q and R^2 values. Q is an empirical attenuation parameter which also includes lateral heterogeneity effects. We further discuss the estimation of the coastal reflection adapted to the area in section 3.2.

2.3. Data

[11] We use 1 year (2010) of continuous waveform data recorded at 20 broadband seismic stations located around the North Atlantic Ocean (Figure 1b): 16 stations (GLISN) are in the Arctic, two stations (CN) are in Quebec and two others (GEOSCOPE) are in France. The data are corrected to ground velocity by removing the instrument response. We use the LH channel (one sample per second) to extract frequency-dependent noise polarization from the continuous three-component records in the 0.05–0.33 Hz frequency band (3–20 s period band).

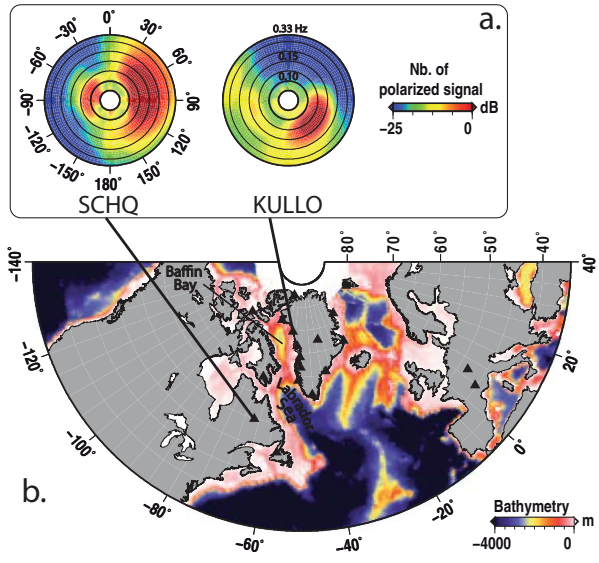

Figure 1. (a) Number of elliptically polarized signals as a function of back azimuth and frequency for two stations, SCHQ (New FoundLand, Canada) and KULLO (North-West Greenland). The source azimuths are plotted as angles with respect to North, and the radius corresponds to the frequencies. The inner and outer circles correspond to frequencies of 0.05 and 0.33 Hz, respectively. A circle is plotted every 0.05 Hz. The bold black circle at 0.1 Hz indicates the probable separation of the two types of microseisms, considering that the maximum energies of the SFM and DFM are, respectively, between 0.05 and 0.1 Hz and above 0.1 Hz. (b) Stations location and ocean bathymetry.

3. Results

3.1. Rayleigh Wave Polarization

[12] For each station, we first analyze yearly averages of the number of Rayleigh waves detected in the noise. Figure 1a shows the number of elliptical polarized signals as a function of back azimuth and frequency for two stations, SCHQ (Schefferville, PQ, New FoundLand, Canada) and KULLO (Kullorsuaq, North-West Greenland). The number of polarized signals was normalized by the maximum count in the year 2010 for each station, i.e., 24,723 for KULLO and 8503 for SCHQ. The source azimuths are plotted as angles with respect to North and the radius corresponds to the frequencies. The inner and outer circles correspond to

frequencies of 0.05 and 0.33 Hz, respectively. A circle is plotted every 0.05 Hz. The bold black circle at 0.1 Hz indicates the likely separation of the two types of microseisms, considering that the maximum energies of the SFM and DFM are, respectively, between 0.05 and 0.1 Hz and above 0.1 Hz [*Schimmel et al*., 2011b].

[13] At the Canadian station SCHQ, most Rayleigh waves come from the East, i.e., from the North Atlantic Ocean (azimuth between 30° and 150°), for frequencies between 0.1 and 0.3 Hz. This frequency range corresponds to the secondary microseisms. Below 0.1 Hz, we observe fewer polarized signals originating from the Atlantic Ocean but we also observe a second direction toward the West, i.e., the Pacific Ocean. These low-frequency Rayleigh waves may be primary microseisms generated along the Pacific coast, secondary microseisms coming from very large Pacific sources or a combination of both. We do not record any signals above 0.15 Hz from the Pacific. It is probable that high-frequency Rayleigh waves corresponding to secondary microseisms are generated in the Pacific, but we expect them to be too strongly attenuated along the path to be recorded by the station in Quebec.

[14] The Greenland station KULLO displays a very different pattern. The main source of Rayleigh waves is toward the Atlantic Ocean (azimuth between 90° and 150°) at frequencies between 0.1 and 0.25 Hz. We also observe weaker sources toward the South and the West at high frequency (0.25–0.33 Hz), and toward the South-West at intermediate frequency (0.15–0.2 Hz). This station seems to record only Rayleigh waves from the Atlantic Ocean and the Labrador Sea.

[15] This analysis of the yearly averaged noise shows that the polarization pattern is frequency dependently different for stations in Canada and Greenland. In the next sections, we shall limit our discussion of noise sources to the secondary microseisms.

3.2. Coastal Reflection Contribution in Noise Source Modeling

[16] We model the noise sources using a numerical ocean wave model [*Ardhuin et al*., 2011]. We determine empirically the ocean wave reflection coefficient R^2 by comparing real and synthetic seismic spectra. At each station, we compute synthetic spectra for wide ranges of R^2 and of the seismic attenuation Q using equation (1). We measure the difference between data and synthetics using correlation and L_1-misfit to analyze the fit in phase and in amplitude. *Ardhuin et al*. [2011] showed on some examples that high correlation between data and synthetic requires different Q and R^2 values per station and frequency band. To investigate the trade-off between the two parameters, we considered the temporal variations of the spectra in different period bands. Data spectra are computed every 6 h over the year 2010. Figures 2 and 3 show the correlation (left-hand side) and misfit (right-hand side) between data and synthetic spectra at two stations in the 7–10 and 3–7 s period bands.

[17] At the Greenland station KULLO, for periods 7–10 s (Figures 2a and 2b), we see that the highest correlation and lowest misfit are achieved for values of attenuation, Q, between 120 and 300 and reflection coefficient, R^2, between 0 and 0.15. We choose the values of Q and R^2 that minimize the misfit, i.e., $Q = 240$ and $R^2 = 0.085$, and we can see on Figure 2e that temporal variations of 7–10 s noise are well modeled. For shorter periods 3–7 s (Figures 2c and 2d), the values of Q vary from 200 to 280 for both correlation and misfit. However, the minimum misfit and highest correlation are achieved for a wide range of R^2 values from 0 to 1. The value of R^2 does not affect 3–7 s noise modeling at KULLO and we choose $R^2 = 0$ for the modeling (Figure 2f).

[18] For the Canadian station SCHQ (Figure 3), in both the 7–10 and 3–7 s period bands, best correlation and lower misfit are obtained for consistent Q values and a very wide range of R^2 from 0 to 1. Temporal variations of seismic noise computed for $R^2 = 0$ generally fit the data. For this station, coastal reflection can be neglected in the short-period seismic noise modeling as well as in the long-period seismic noise modeling.

[19] The comparison between data and synthetic spectra at every station shows that the value of R^2 does not affect the misfit for periods shorter than 7 s. Any R^2 value between 0 and 1 fits the data equivalently. The ocean wave reflection coefficient is not well constrained. Varying this coefficient does not change significantly either the noise spectra modeling or the amplitude of noise sources in this period range in the North Atlantic. As the sources maps in the North Atlantic are similar whatever the reflection coefficient, we model seismic sources with $R^2 = 0$ in the 3–4 and 4–7 s period bands. Figure 4a shows the distribution of coastal reflection coefficient R^2 obtained for each

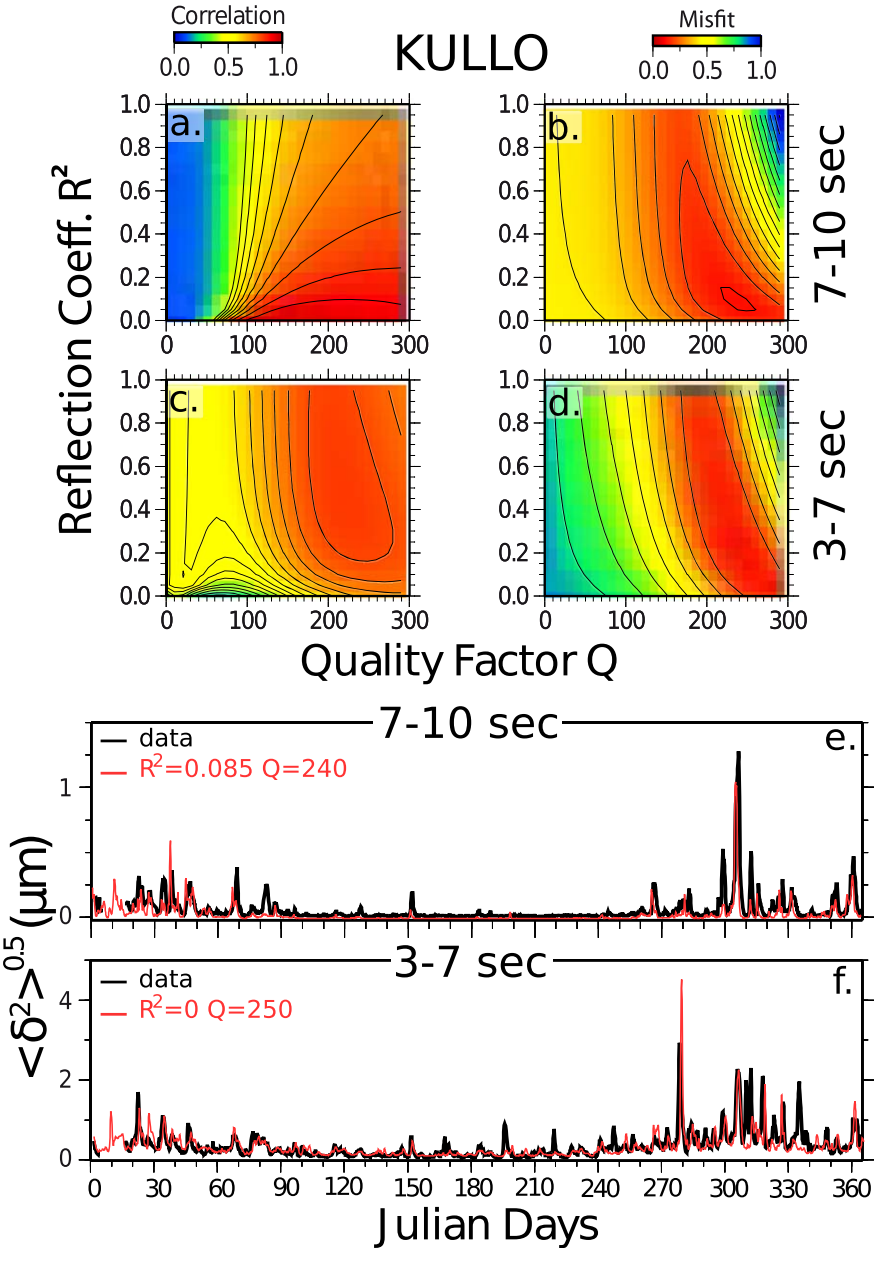

Figure 2. Seismic noise modeling for station KULLO (Western Greenland). (a and c) Correlation and (b and d) misfit between real and synthetic spectra as a function of seismic attenuation Q and ocean wave coastal reflection coefficient R^2 in two period bands 7–10 s (Figures 2a and 2b) and 3–7 s (Figures 2c and 2d). Real (black) and synthetic (red) spectra variations over 1 year in displacement averaged over period bands (e) 7–10 s and (f) 3–7 s. The synthetic spectra (red) are computed for (Q, R^2) values that minimize the misfit and compared to the data (black).

station in the period band 7–10 s. Blue crosses indicate the stations for which the lowest misfit between data and synthetics are achieved for any R^2 value. For 7–10 s source modeling, we use the coefficient obtained at most stations, i.e., $R^2 = 6.25\%$ (Figure 4b).

[20] The exact value of R^2 is not well constrained but it cannot be zero to model the 7–10 s noise sources. We show the secondary microseism sources modeled in the 7–10 s period band with $R^2 = 0$ in Figure 5 and $R^2 = 6.25\%$ in Figures 6a and 6d. We show the averaged sources for two 1 month periods, the first in March 2010 (left-hand side) when the ice cover is at its largest extent and the second in September 2010 (right-hand side) when it is at its smallest extent. We can see differences between sources modeled with and without ocean wave coastal reflection. In March, the amplitude of sources in the Pacific and at the tip of Greenland

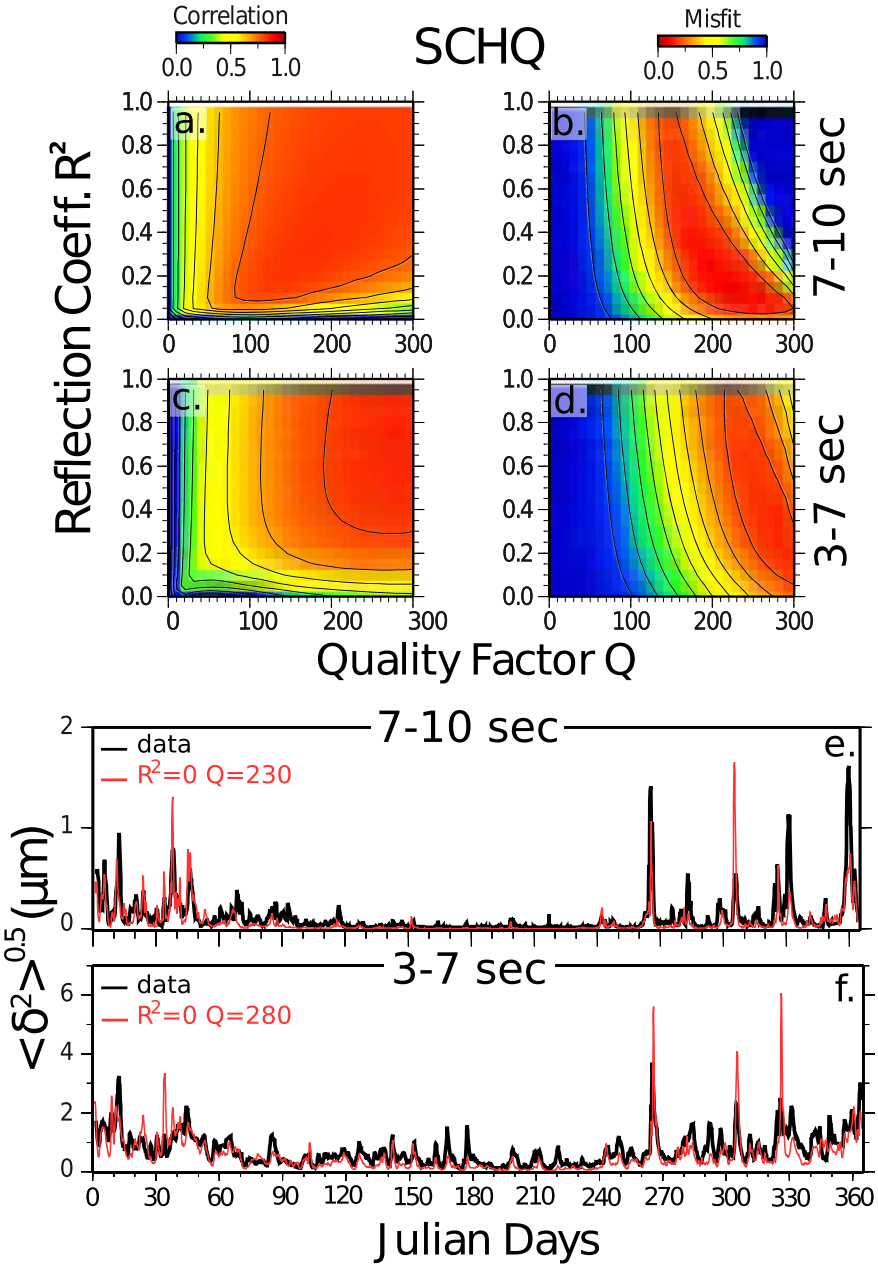

Figure 3. Seismic noise modeling for station SCHQ (New FoundLand, Canada). Same as for Figure 2.

is much stronger when the sources of class II (interaction of incident and coastal reflected waves) are modeled (Figure 6a). In September, we observe the appearance of new class II sources at the tip of Greenland and in the Labrador Sea (Figure 6d) that we do not see on source maps modeled with $R^2 = 0$ (Figure 5b). We further show in the next section that 7–10 s sources modeled with $R^2 = 6.25\%$ may well explain noise recorded at stations around North Atlantic.

3.3. Frequency-Dependent Noise Sources

[21] We compare here the sources associated with the secondary microseism Rayleigh waves detected by our polarization analysis. Figure 6 shows the modeled DFM sources in the period bands 7–10 s (0.1–0.15 Hz), 4–7 s (0.15–0.25 Hz), and 3–4 s (0.25–0.33 Hz) for March and September 2010. As discussed previously, we adjust the ocean wave coastal reflection as a function of period and use $R^2 = 6.25\%$ for seismic periods 7–10 s and $R^2 = 0\%$ for seismic periods 4–7 and 3–4 s. We also plot for each station the source azimuth determined from the polarization analysis in angular histograms. We only plot the polarization results for the 10 stations that were available for both months in 2010. The number of back

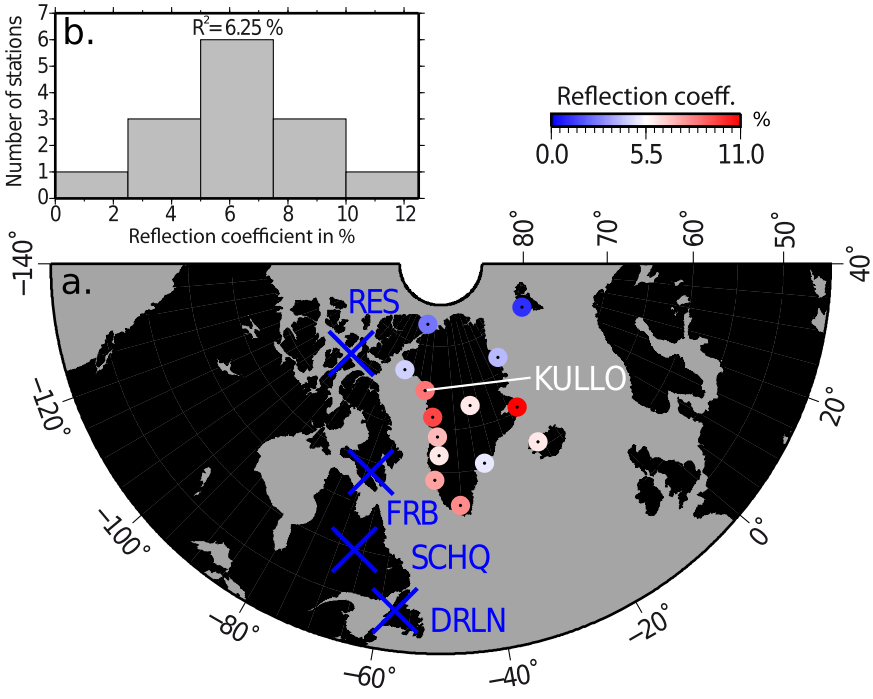

Figure 4. (a) Distribution of the ocean wave reflection coefficient R^2 that minimizes the misfit between the real and synthetic power spectra at each station for period band 7–10 s. The blue crosses indicate the stations for which the value of R^2 have no effect on the misfit. (b) Histogram of the number of stations in Greenland for each R^2 value in percent.

azimuths is compiled in angular histograms whose vectors point toward the measured back azimuths. The different scales show that fewer short-period Rayleigh waves were detected than longer-period waves. This may be due to changes of the relative excitation of the fundamental and the higher modes at short period related to changes of the bathymetry at the source location [*Tanimoto et al.*, 2006]. This effect is larger at short period and the measured azimuths at 3–4 s may be less accurate than the longer-period azimuths.

[22] The main directions observed at individual stations generally point toward the modeled sources. The frequency dependence of the back azimuths can be explained by the frequency dependence of the source locations. In March, the strongest long-period (7–10 s) sources are in the Pacific and in the mid-Atlantic (Figure 6a). The four Canadian stations record predominantly the strong Pacific sources. Stations in Greenland, Iceland, and Europe record Rayleigh waves from the mid-Atlantic sources and sources on either side of the ridge South of Iceland. The comparison between this map and Figure 5a shows that the strong amplitude of the class II sources in the North Pacific and near the Southern tip of Greenland may well explain the strong polarization of 7–10 s noise recorded at Canadian, Greenland, and Iceland stations.

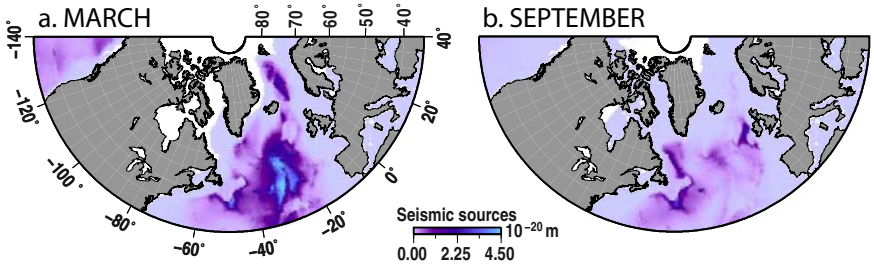

Figure 5. The 7–10 s secondary microseism sources in (a) March and (b) September modeled without ocean wave coastal reflections ($R^2 = 0\%$). The color maps show the corresponding modeled sources and the ice floe is represented by the white areas.

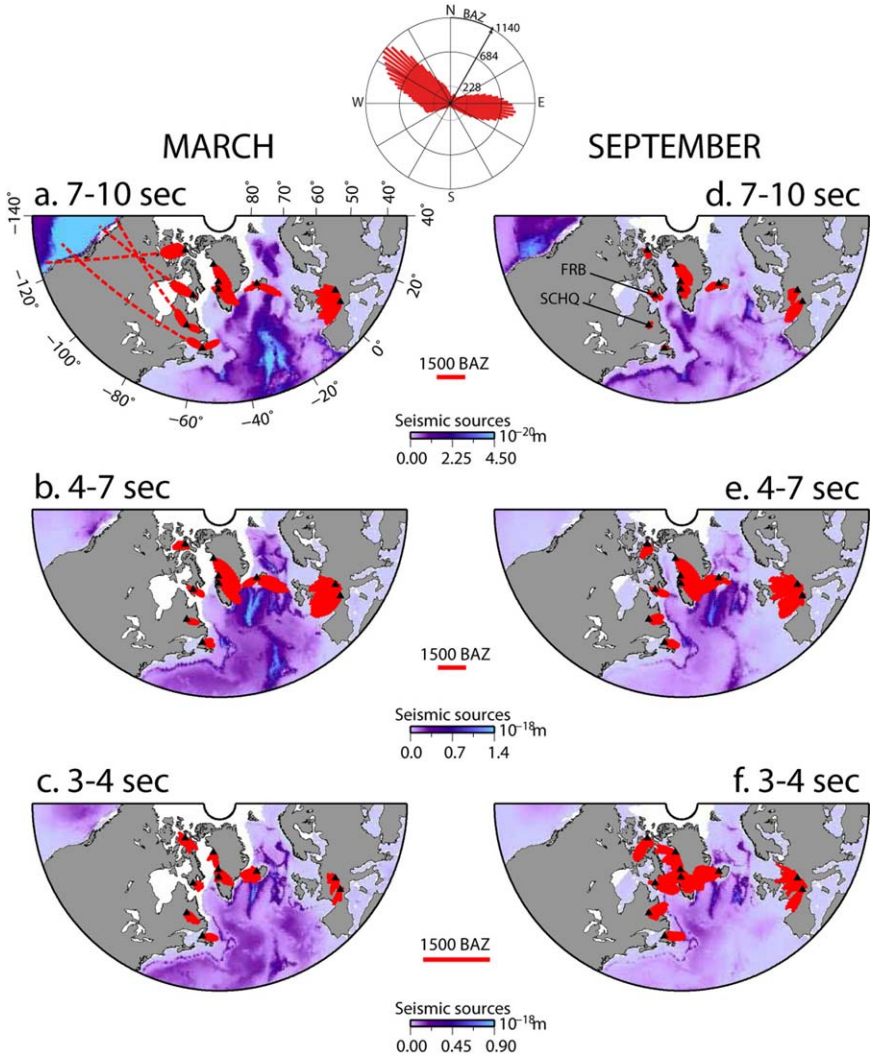

Figure 6. Distributions of the secondary microseism sources in (left) March and (right) September in three different period bands: (a and b) 7–10 s, (c and d) 4–7 s, and (e and f) 3–4 s. The color maps show the corresponding modeled sources and the ice floe is represented by the white areas. The sources are modeled using a coastal reflection of 6.25% for 7–10 s period band. At each station, the number of back azimuths is compiled in angular histograms. The different scales show that less short-period Rayleigh waves were detected than longer-period waves. The red dotted lines show the great circle path from stations in Canada along the dominant back azimuth. Stations are plotted with triangles.

[23] At shorter periods (4–7 s, Figure 6c), the strongest sources are in the Atlantic Ocean in the vicinity of the ridge axis close to Iceland and to the Azores, i.e., in a different location than the longer-period sources. We note also the emergence of smaller amplitude sources near the Canadian coast. Greenland stations record sources toward the South East which can be either at the tip of Greenland or further away to the South of Greenland near the ridge axis. The Iceland station records source azimuths that seem to correspond to sources close to Greenland. At even shorter period (3–4 s, Figure 6e), the strongest deep ocean sources have moved again and are now right on the ridge axis close to Iceland. Greenland stations record signals coming from the Labrador Sea and South of Greenland. The Iceland station records source azimuths that correspond to sources along the Greenland coast and at the ridge axis.

[24] In September, the strongest long-period sources (7–10 s, Figure 6b) are in the Pacific Ocean and along the coasts. We also observe sources close to Ireland which are much stronger than those observed in March. The Canadian stations record very few Rayleigh waves and almost none

from the Pacific direction. All the stations record Rayleigh waves from the Atlantic sources. We also note that sources along the Canadian coast, in the Labrador Sea and at the tip of Greenland are coastal (class II sources) as they do not appear in Figure 5b. Their presence explains well the source azimuths at Canadian stations FRB and SCHQ, Greenland and Iceland stations. In the 4–7 s period band (Figure 6d) there are no significant seasonal variations in Rayleigh wave polarizations or source locations. We observe the dominant and constant source near the southern tip of Greenland that has been reported by previous studies [*Kedar et al.*, 2008; *Ardhuin et al.*, 2011; *Stutzmann et al.*, 2012]. At the shortest periods (3–4 s), the most striking observation is that stations in Greenland and Canada record sources from the Labrador Sea and Baffin Bay (West of Greenland) that can be related to the seasonal withdrawal of the ice floe. The relationship between seismic noise and sea-ice is investigated in more detail in the next section.

[25] We extract between 5000 and 25,000 polarized signals at individual stations throughout the year. The number of polarized signals varies from station to station. The highest numbers of polarized signals are detected at stations on the West coast of Greenland. Stations in Canada and Iceland detect fewer polarized signals. In Figures 6a, 6b, 6d, and 6e, we observe that Canadian stations record fewer polarized signals coming from the direction of the Atlantic than stations in Greenland and Europe. The Canadian stations seem to record either Rayleigh waves generated close to nearby coasts, those generated near the Southern tip of Greenland or those generated along the mid-Atlantic ridge. It may be difficult to extract a clear polarized signal from the interference of these Rayleigh waves. Similarly, the station in Iceland records Rayleigh waves coming from the South-West and the South-East, and very few signals from the Southern direction that point toward the ridge where we observe strong sources in the model. The large spatial extent of this source may distort the polarization, which then would not be detected by our procedure.

4. Sea-Ice Effect on the Seasonal Variations of the Secondary Microseisms

[26] To investigate the influence of ice cover on the secondary microseisms in the Labrador Sea, we analyze noise spectral density and polarization variations over the year 2010 for station FRB (Iqaluit, NU) located in Baffin Island, Canada.

[27] Both the noise spectrogram (PSD) and the normalized number of polarized signal (NPS) display seasonal variations that are frequency dependent (Figures 7a and 7b). For frequencies between 0.1 and 0.2 Hz (5–10 s), noise amplitude is weaker in summer (Julian days 100–260) than in winter as already observed by many authors [*Bromirski et al.*, 1999; *Stutzmann et al.*, 2000; *Aster et al.*, 2008; *Stutzmann et al.*, 2009]. However, above 0.2 Hz (period 3–5 s), amplitude and number of polarized signals are higher during summer and autumn (Julian days 170–355). Figure 7c shows the variations of the number of polarized signals for frequencies between 0.2 and 0.33 Hz, as a function of time and back azimuth. They are counted in nonoverlapping bins of 1 day × 3°. We see that Rayleigh waves arrive at FRB from a constant direction between 60° and 150° throughout the year, but that more polarized signals are detected during the second part of the year as already observed in Figure 7b. We also note the appearance of a new direction of incoming waves (200°/220°) around day 210, which remains present during the second part of the year. This implies the existence of noise sources West of the station that are quiescent until July 2010. Figure 7d shows the temporal variations of the sea-ice concentration (data collected from NSIDC) as a function of distance along a 500 km profile starting from FRB and pointing toward the nearest ice-free sea (Labrador Sea). We only represent the last 225 km of the profile as the station is inland from the coast. We observe a good correlation between (a) the rise of 0.2–0.33 Hz microseism level and the number of detected Rayleigh waves (Figures 7a and 7b), (b) the excitation of new and/or more numerous 0.2–0.33 Hz sources (Figure 7c), and (c) the disappearance of sea-ice around the station. This correlation is summarized in Figure 7e.

[28] Figures 7f–7i show the modeled sources averaged over March and September 2010 in two frequency bands: 0.25–0.33 Hz (3–4 s) and 0.2–0.25 Hz (4–5 s). We also plot the angular histograms of polarization analysis at four stations in the corresponding frequency bands. At FRB, the number of polarized signals for the 3–4 s period band is higher in September than in March (Figures 7g and 7f) as already observed in Figure 7b. We also observe the appearance of new westward BAZs at FRB in September. Since short-period microseisms do not propagate efficiently over large

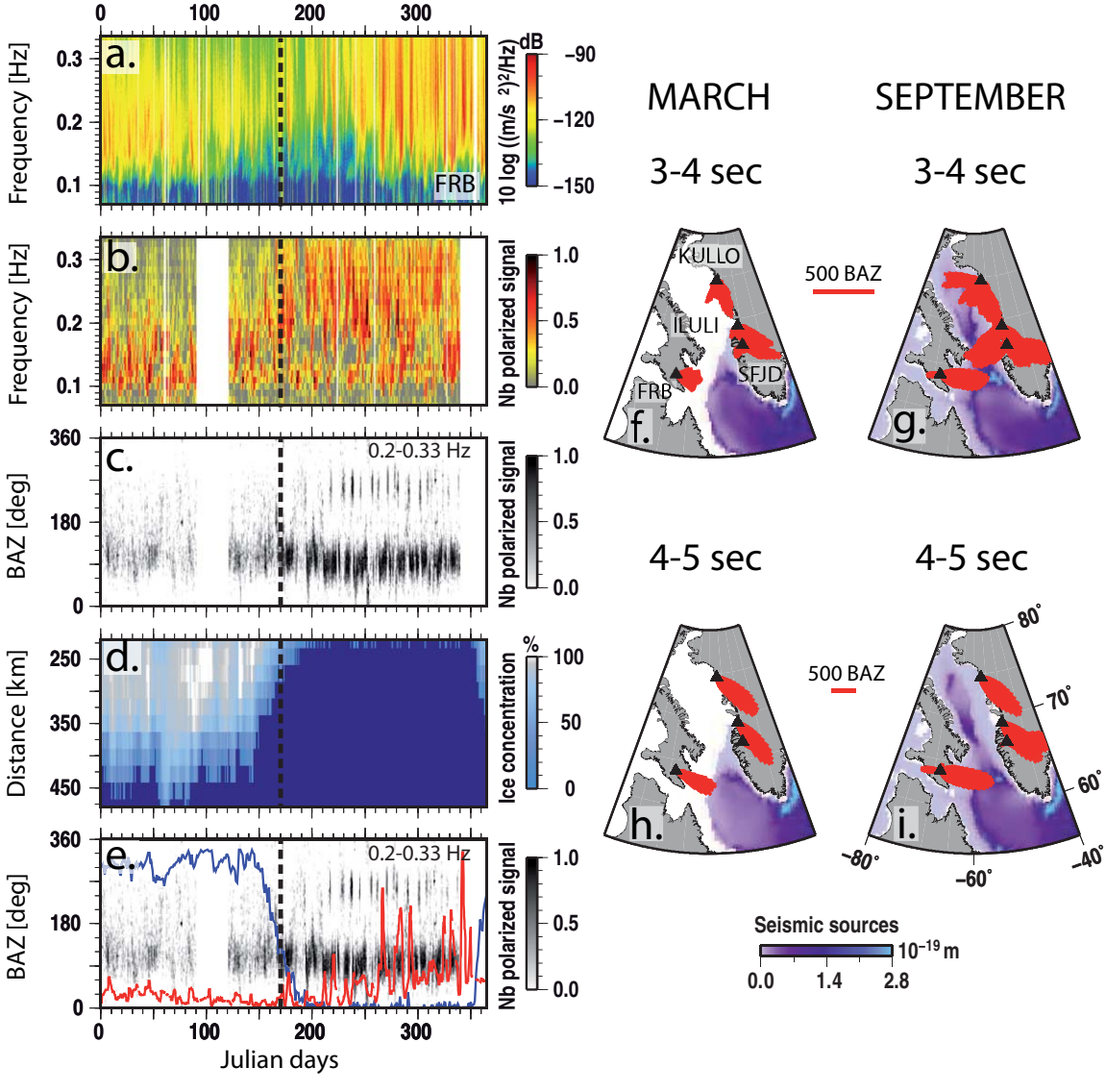

Figure 7. Left: For station FRB, (a) seismic noise spectrogram over the year 2010 in dB. (b) Normalized number of polarized signals over the year 2010 as a function of time and frequency. (c) Number of polarized signal in the frequency band 0.2 and 0.33 Hz as a function of time and back azimuth. (d) Temporal variation of the sea-ice concentration as a function of distance along a 500 km profile starting from FRB and pointing toward the nearest ice-free sea. (e) Synthesis of the previous figures: for the period band 0.2–0.33 Hz, is plotted the number of polarized signal (black points), the noise spectrum (red), and the sea-ice-free distance (blue). Right: Distributions of the secondary microseism sources in (left) March and (right) September in the period band (f and g) 4–5 s and (h and i) 3–4 s. Angular histograms at each station show the back azimuths.

distances [*Bromirski et al.*, 2005], we interpret these 3–4 s Rayleigh waves as coming from local sources somewhere in the ice-free sea West of the station, even though such sources are not observed in our model. For all stations in Greenland, the source azimuths in the period band 4–5 s point consistently toward South-East Greenland (Figures 7h and 7i), and never point toward the Labrador Sea even when it is ice free. It is only at short periods (3–4 s) that these stations record Rayleigh waves from the South of Greenland and from the Labrador Sea and Baffin Bay (Figure 7f).

[29] Several studies have reported the influence of sea-ice on the amplitude of seismic noise spectra recorded at stations in Antarctic [*Stutzmann et al.*, 2009; *Grob et al.*, 2011] and Arctic [*Harben and Hjortenberg*, 1993; *Kedar et al.*, 2008; *Tsai and McNamara*, 2011]. In the Arctic, *Kedar et al.* [2008] first showed that the sea-ice edge in the

Labrador Sea is a necessary parameter to model the noise spectra accurately. They averaged their spectra in the entire frequency range of the secondary microseisms 3–7 s. Here, we show that in 2010, the sea-ice in the Labrador Sea only modifies the short-period seismic noise (periods smaller than 4 s) in agreement with the source model that shows no strong longer-period source in the area and in Baffin Bay (Figures 6d and 6e).

5. Conclusions

[30] Seismic noise polarization analysis and noise source modeling show consistent frequency-dependent patterns in the North Atlantic. Coastal reflection is taken into account in our ocean wave modeling and its values are adjusted by comparing real and synthetic spectra. This comparison shows that coastal reflection can be neglected for periods smaller than 7 s and is around 6% for longer periods. *Kedar et al*. [2008] first showed the existence of a strong source South of Greenland in November 2003, using a wave model that does not take the reflection coefficient into account. They averaged their result in the seismic period band 3–7 s, for which coastal reflection can indeed be neglected, to explain the data. Our results are consistent with their study in that period band. We further show the existence of other sources along the Canadian coast and close to the mid-Atlantic ridge. The sources near the ridge are closer to Iceland for the periods 4–7 s than for 3–4 s. These source variations with period are consistent with the source azimuth variations observed at stations in Iceland and Greenland and are related to the complex excitation of noise sources. Indeed the source amplitude depends on the ocean wave amplitude which varies with time and frequency. Furthermore, the seismic waves generated at a given location in the ocean are modulated as a function of frequency, local water depth, and crustal S-wave velocity [*Longuet-Higgins*, 1950]. *Stutzmann et al*. [2012] showed the existence of different source amplification areas with period. Here, we show the variability of DFM sources in the North Atlantic with period by combining source modeling and Rayleigh wave polarization analysis at nearby stations.

[31] Zooming in the Labrador Sea and Baffin Bay, we show the existence of short-period (3–4 s) noise sources when the sea is not covered by sea-ice. Sea-ice modifies both the amplitude and the polarization of the noise recorded by stations nearby. The influence of sea-ice in the Labrador Sea on seismic noise was first reported by *Kedar et al*. [2008]. Here, we further show that it only affects seismic noise in the period band 3–4 s at nearby stations, which is consistent with the absence of long-period sources in these regions. The absence of long-period sources can be explained by the small extent of the sea which makes difficult to develop long-period ocean waves, and by the shallow bathymetry which decreases long-period source amplitude with respect to shorter-period sources.

[32] Finally, we show that coastal reflection of the ocean waves must be taken into account for modeling the long-period noise sources, and that the resulting sources are consistent with the source azimuths derived from the polarization analysis. Stations in North Canada record North Pacific sources generated by coastal reflection in March and very few Atlantic sources in September. The other stations only record sources toward the Atlantic Ocean.

[33] This study illustrates the complexity of the microseismic noise recorded by seismic stations in the North Atlantic, which is due to the frequency-dependent pattern of the noise sources and the sea-ice changes.

Acknowledgments

[34] We thank the operators of GEOSCOPE and IRIS/IDA for providing the broadband seismic data used in this study. Data were taken from both GEOSCOPE and IRIS data centers. We have used data from the following networks: CN (Canadian National Seismograph Network), DK (Danish Seismological Network), G (GEOSCOPE), GE (GEOFON), II, and IU. Wind and wave data were provided by ECMWF, and wave buoy data were taken from the U.S. National Data Buoy Center and the Coastal Data Information Program. The daily gridded sea-ice concentrations were taken from NSIDC (National Snow and Ice Data Center). We thank Aurélien Mordret for his suggestions on an early version of this paper. M.S. acknowledges financial support by the projects Rifsis (CGL 2009–09727) and TopoIberia (CSD2006-00041). This is IPGP contribution 3449.

References

Anderson, K., et al. (2009), The Greenland ice sheet monitoring network (GLISN), American Geophysical Union, Fall Meeting 2009, abstract U51C-0032.

Ardhuin, F., E. Stutzmann, M. Schimmel, and A. Mangeney (2011), Ocean wave sources of seismic noise, *J. Geophys. Res.*, *116*, C09004, doi:10.1029/2011JC006952.

Ardhuin, F., A. Balanche, E. Stutzmann, and M. Obrebski (2012), From seismic noise to ocean wave parameters: General methods and validation, *J. Geophys. Res.*, *117*, C05002, doi:10.1029/2011JC007449.

Aster, R., D. McNamara, and P. Bromirski (2008), Multidecadal climate-induced variability in microseisms, *Seismol. Res. Lett.*, *79*(2), 194–202.

Aster, R., D. McNamara, and P. Bromirski (2010), Global trends in extremal microseism intensity, *Geophys. Res. Lett.*, *37*, L14303, doi:10.1029/2010GL043472.

Behr, Y., J. Townend, M. Bowen, L. Carter, R. Gorman, L. Brooks, and S. Bannister (2013), Source directionality of ambient seismic noise inferred from three-component beamforming, *J. Geophys. Res. Solid Earth*, *118*, 240–248, doi:10.1029/2012JB009382.

Bromirski, P. D., and F. K. Duennebier (2002), The near-coastal microseism spectrum: Spatial and temporal wave climate relationships, *J. Geophys. Res.*, *107*(B8), 2166, doi:10.1029/2001JB000265.

Bromirski, P., R. Flick, and N. Graham (1999), Ocean wave height determined from inland seismometer data: Implications for investigating wave climate changes in the NE Pacific, *J. Geophys. Res.*, *104*, 20,753–20,766.

Bromirski, P., F. Duennebier, and R. Stephen (2005), Mid-ocean microseisms, *Geochem. Geophys. Geosyst.*, *6*, Q04009, doi:10.1029/2004GC000768.

Bromirski, P. D., R. A. Stephen, and P. Gerstoft (2013), Are deep-ocean-generated surface-wave microseisms observed on land?, *J. Geophys. Res. Solid Earth*, *118*, 3610–3629, doi:10.1002/JGRB.50268.

Brooks, L. A., J. Townend, P. Gerstoft, S. Bannister, and L. Carter (2009), Fundamental and higher-mode Rayleigh wave characteristics of ambient seismic noise in New Zealand, *Geophys. Res. Lett.*, *36*, L23303, doi:10.1029/2009GL040434.

Cessaro, R. (1994), Sources of primary and secondary microseisms, *Bull. Seismol. Soc. Am.*, *84*(1), 142–148.

Chevrot, S., M. Sylvander, S. Benahmed, C. Ponsolles, J. Lefèvre, and D. Paradis (2007), Source locations of secondary microseisms in western Europe: Evidence for both coastal and pelagic sources, *J. Geophys. Res.*, *112*, B11301, doi:10.1029/2007JB005059.

Friedrich, A., F. Kruger, and K. Klinge (1998), Ocean-generated microseismic noise located with the Grafenberg array, *J. Seismol.*, *2*(1), 47–64.

Gerstoft, P., and T. Tanimoto (2007), A year of microseisms in southern California, *Geophys. Res. Lett.*, *34*, L20304, doi:10.1029/2007GL031091.

Grob, M., A. Maggi, and E. Stutzmann (2011), Observations of the seasonality of the Antarctic microseismic signal, and its association to sea ice variability, *Geophys. Res. Lett.*, *38*, L11302, doi:10.1029/2011GL047525.

Gualtieri, L., E. Stutzmann, Y. Capdeville, F. Ardhuin, M. Schimmel, A. Mangeney, and A. Morelli (2013), Modelling secondary microseismic noise by normal mode summation, *Geophys. J. Int.*, *193*(3), 1732–1745.

Harben, P., and E. Hjortenberg (1993), Variation in microseism power and direction of approach in northeast Greenland, *Bull. Seismol. Soc. Am.*, *83*(6), 1939–1958.

Hasselmann, K. (1963), A statistical analysis of the generation of microseisms, *Rev. Geophys.*, *1*, 177–210.

Kedar, S., M. Longuet-Higgins, F. Webb, N. Graham, R. Clayton, and C. Jones (2008), The origin of deep ocean microseisms in the north Atlantic Ocean, *Proc. R. Soc. A*, *464*(2091), 777–793.

Koper, K., K. Seats, and H. Benz (2010), On the composition of earths short-period seismic noise field, *Bull. Seismol. Soc. Am.*, *100*(2), 606–617.

Longuet-Higgins, M. (1950), A theory of the origin of microseisms, *Philos. Trans. R. Soc. London A*, *243*(857), 1–35.

Obrebski, M., F. Ardhuin, E. Stutzmann, and M. Schimmel (2012), How moderate sea states can generate loud seismic noise in the deep ocean, *Geophys. Res. Lett.*, *39*, L11601, doi:10.1029/2012GL051896.

Schimmel, M., and J. Gallart (2004), Degree of polarization filter for frequency-dependent signal enhancement through noise suppression, *Bull. Seismol. Soc. Am.*, *94*, 1016–1035.

Schimmel, M., E. Stutzmann, and J. Gallart (2011a), Using instantaneous phase coherence for signal extraction from ambient noise data at a local to a global scale, *Geophys. J. Int.*, *184*, 494–506.

Schimmel, M., E. Stutzmann, F. Ardhuin, and J. Gallart (2011b), Polarized Earth's ambient microseismic noise, *Geochem. Geophys. Geosyst.*, *12*, Q07014, doi:10.1029/2011GC003661.

Schulte-Pelkum, V., P. Earle, and F. Vernon (2004), Strong directivity of ocean-generated seismic noise, *Geochem. Geophys. Geosyst.*, *5*, Q03004, doi:10.1029/2003GC000520.

Stehly, L., M. Campillo, and N. Shapiro (2006), A study of the seismic noise from its long-range correlation properties, *J. Geophys. Res.*, *111*, B10306, doi:10.1029/2005JB004237.

Stockwell, R., L. Mansinha, and R. Lowe (1996), Localization of the complex spectrum: The S transform, *IEEE Trans. Signal Process.*, *44*(4), 998–1001.

Stutzmann, E., G. Roult, and L. Astiz (2000), Geoscope station noise levels, *Bull. Seismol. Soc. Am.*, *90*(3), 690–701.

Stutzmann, E., M. Schimmel, G. Patau, and A. Maggi (2009), Global climate imprint on seismic noise, *Geochem. Geophys. Geosyst.*, *10*, Q11004, doi:10.1029/2009GC002619.

Stutzmann, E., F. Ardhuin, M. Schimmel, A. Mangeney, and G. Patau (2012), Modelling long-term seismic noise in various environments, *Geophys. J. Int.*, *191*(2), 707–722.

Tanimoto, T., S. Ishimaru, and C. Alvizuri (2006), Seasonality in particle motion of microseisms, *Geophys. J. Int.*, *166*(1), 253–266.

Tsai, V., and D. McNamara (2011), Quantifying the influence of sea ice on ocean microseism using observations from the Bering Sea, Alaska, *Geophys. Res. Lett.*, *38*, L22502, doi:10.1029/2011GL049791.

Ventosa, S., C. Simon, M. Schimmel, J. Danobeitia, and A. Manuel (2008), The s-transform from a wavelet point of view, *IEEE Trans. Signal Process.*, *56*(7), 2771–2780.